Continental Shelf Research 188 (2019) 103963

Contents lists available at ScienceDirect

Continental Shelf Research

journal homepage: www.elsevier.com/locate/csr

Research papers

Impact of cage aquaculture on water exchange in Sansha Bay

Hongyang Lin[a], Zhaozhang Chen[a,*], Jianyu Hu[a], Andrea Cucco[b], Zhenyu Sun[a], Xirong Chen[a], Lingfeng Huang[c]

[a] State Key Laboratory of Marine Environmental Science, College of Ocean and Earth Sciences, Xiamen University, Xiamen, Fujian, 361102, China
[b] Institute for Study of Anthropic Impacts and Sustainability in Marine Environment, CNR-IAS, TorreGrande, 09170, Oristano, Italy
[c] College of the Environment and Ecology, Xiamen University, Xiamen, Fujian 361102, China

ARTICLE INFO

Keywords:
Sansha bay
Cage aquaculture
Cage-induced drag
Water exchange
Hydrodynamic model

ABSTRACT

Influence of cage aquaculture on the flow field and water exchange in Sansha Bay is investigated based on *in situ* current measurements and output from a two-dimensional shallow water hydrodynamic finite element model (SHYFEM). Without cage influence, the flow is relatively uniform in the vertical except a bottom Ekman layer. An asymmetry of tidal current speed is also observed in Sansha Bay with a dominance of the ebb tide. Near-surface current speed squared in cage-free area is typically larger than that within cage area by a factor exceeding three in deep channels, and by a factor of two in tidal flats. Current speed profiles suggest that cage-induced drag on the flow field can reach as deep as 20 m in the relatively deep channels of Sansha Bay. A set of numerical experiments are designed to quantify the relative effect of cages in tidal flats and channels, respectively, on water exchange using SHYFEM. It is shown that cage aquaculture weakens the local flow but seems to strengthen the flow adjacent to cages. Reducing the frictional drag in channels significantly increases the water exchange rate both locally and in the near-field tidal flats. Therefore, certain clearance or rearrangement of cage aquaculture in channels would be more effective in improving the water exchange in the entire Sansha Bay.

1. Introduction

Aquaculture is expanding rapidly in recent years, and serves as an important component of the global food production (Edwards, 2015; Weitzman et al., 2019). However, the rapid growth has also caused a number of ecological and socioeconomical issues (e.g., Holmer et al., 2005; Naylor et al., 2000). For example, the aquaculture feed is a conspicuous source of organic loading to the local marine environment; there are also conflicts of space and resources between aquaculture activities and other marine uses. Although aquaculture also exists and is expanding at offshore areas, most of the activities are operated near-shore, in particular, within cages. As summarized by Weitzman et al. (2019), marine cage farming could potentially i) have impacts on the local benthic communities due to the sinking of released particulate matter to seafloor, ii) affect the ambient water quality by changing the physiochemical properties of the water column through discharge of particulate and dissolved compounds, and iii) modify the surrounding habitat because the physical structures (e.g., floats, submerged nets) used to construct cages would inevitably influence light penetration, local currents, ecological habitats, etc.

Impact of cage aquaculture on the surrounding marine environment has been studied extensively, in the context of impacts from different perspectives and in various coastal regions over the world (e.g., Holmer et al., 2002; Shi et al., 2011; Ferreira et al., 2014). Based on available observations and a particle tracking model, San Diego-McGlone et al. (2008) examined the influence of fish pens and cages on the surrounding water quality in the waters of Bolinao, Pangasinan, Philippines. They found that in addition to the organic loading that deteriorated the water quality, the presence of excessive fish pens and cages in the shallow embayment attenuated local currents (or flushing rate) leading to longer water residence time which further exacerbated the water quality. Herrera et al. (2018) proposed a modeling framework to assess the interactions between local hydrodynamics and salmon cages and applied it to the Estero Elefantes Channel, Chile, as a study case. They argued that cages not only modified the local hydrodynamics of the channel by slowing down the water exchange, but also had a far-field effect because of the propagation of cage-induced perturbations. Interactions between mariculture and hydrodynamics have also been studied in many coastal regions of China (e.g., Shi and Wei, 2009; Shi et al., 2011). For example, Shi and Wei (2009) simulated the hydrodynamics of Sanggou Bay, a semi-enclosed embayment in the eastern Shandong, China, considering the frictional drag caused by the

* Corresponding author.
E-mail address: zzchen@xmu.edu.cn (Z. Chen).

https://doi.org/10.1016/j.csr.2019.103963
Received 21 December 2018; Received in revised form 30 June 2019; Accepted 29 August 2019
Available online 10 September 2019
0278-4343/

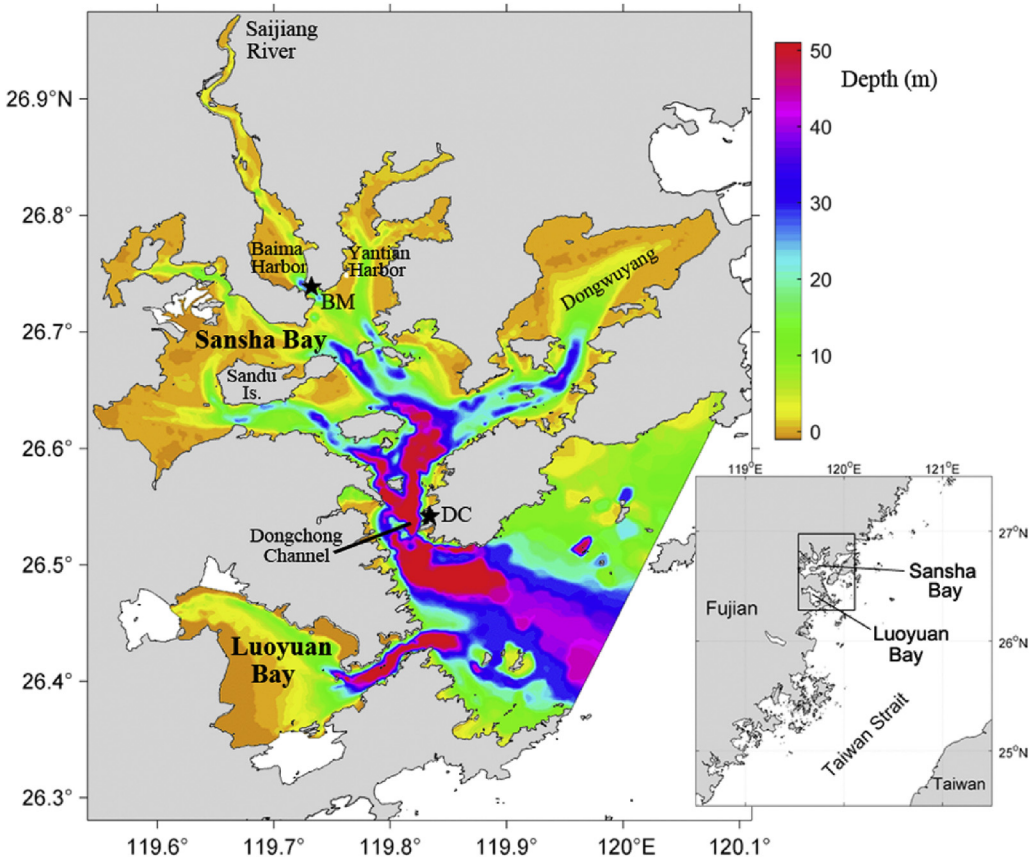

Fig. 1. Bathymetry of Sansha Bay with the main islands, harbors and channels labeled. The lower right inset shows the location of Sansha Bay. The two black stars denote the water-level station at Dongchong (DC) and Baima (BM).

mariculture facilities and cultured species.

This study aims to study the impact of cage aquaculture on the local hydrodynamics in Sansha Bay, a semi-enclosed bay in the northeastern area of Fujian, China. Sansha Bay consists of several secondary bays such as Baima Harbor, Yantian Harbor, Dongwuyang and Guanjingyang (see Fig. 1 for locations). Sansha Bay has a relatively large water area of approximately 675 km^2, but there is only one narrow gateway (i.e., Dongchong Channel) of approximately 3-km wide in the south bridging the bay and the outer waters (i.e., the Taiwan Strait). The water quality and ecosystem of the bay have been degrading in recent years (Wu et al., 2012; Sun et al., 2015). Part of the reason is the increasing cage aquaculture in Sansha Bay over the past decade, which could deteriorate the water quality from two aspects. Biologically, cage aquaculture has been demonstrated to increase the concentration of nutrients (e.g., dissolved inorganic nitrogen, active phosphorus) and also to reduce species number and diversity in Sansha Bay (e.g., Liu et al., 2003; Zhu et al., 2013; Shen et al., 2014; Sun et al., 2015). Physically, nets and cages would naturally slow down the movement of sea water by increasing the frictional drag (Klebert et al., 2013; Weitzman et al., 2019), and hence retard water exchange between the bay and outer waters. Using current meter measurements, Jackson and Winant (1983) found that the magnitudes of ocean currents outside a kelp forest were three times greater than those inside, demonstrating the drag induced by such marine plants. Based on observations and model output, Udarbe-Walker and Magdaong (2003) reported that current speed inside the cultured structures reduced by approximately 30–60% compared to that outside. This study aims to examine the influence of cage aquaculture on water exchange in Sansha Bay using *in situ* current measurements and model simulations with a set of sensitivity runs.

The manuscript is structured as follows. Section 2 describes the study region including the regional physical oceanography and the distribution of cages in Sansha Bay. The observations and model configurations are briefly introduced in Section 3. The observed impact of the cage-induced drag on the local water exchange is examined in Section 4, whereas the simulated impact with different sensitivity runs is investigated in Section 5. Section 6 includes the conclusions and discussion.

2. Study area

2.1. Regional physical oceanography

We will briefly introduce the regional physical oceanography in this section. Given the unique morphology (relatively large area with a narrow gateway), Sansha Bay is a natural sheltered bay for fishing vessels during heavy weather conditions (Wang et al., 2009). Under the influence of river runoff, the bay head is characterized by high-temperature and low-salinity water, whereas low-temperature and high-salinity water occupies the bay mouth (Lin et al., 2016). The temperature difference between bay head and mouth is smaller in winter than in summer, probably due to the seasonal variation of solar radiation. The bay head-mouth difference in salinity is also smaller in winter, possibly due to the southward deflection of the fresh China Coast Current which enters Sansha Bay with the help of flood tides (Lin et al., 2016). With regard to the local tides, the water-level variability in Sansha Bay is dominated by regular semi-diurnal tides (Lin et al., 2017b). The local currents are also significantly affected by tides with the magnitude of tidal currents exceeding 1 $m\,s^{-1}$ in deep areas (e.g., channels) but less than 0.5 $m\,s^{-1}$ in shallow areas (e.g., tidal flats). If the tides are removed, the residual currents are much weaker without a clear current direction (Lin et al., 2017a). The residual water level is in good correspondence with alongshore winds, while the difference of

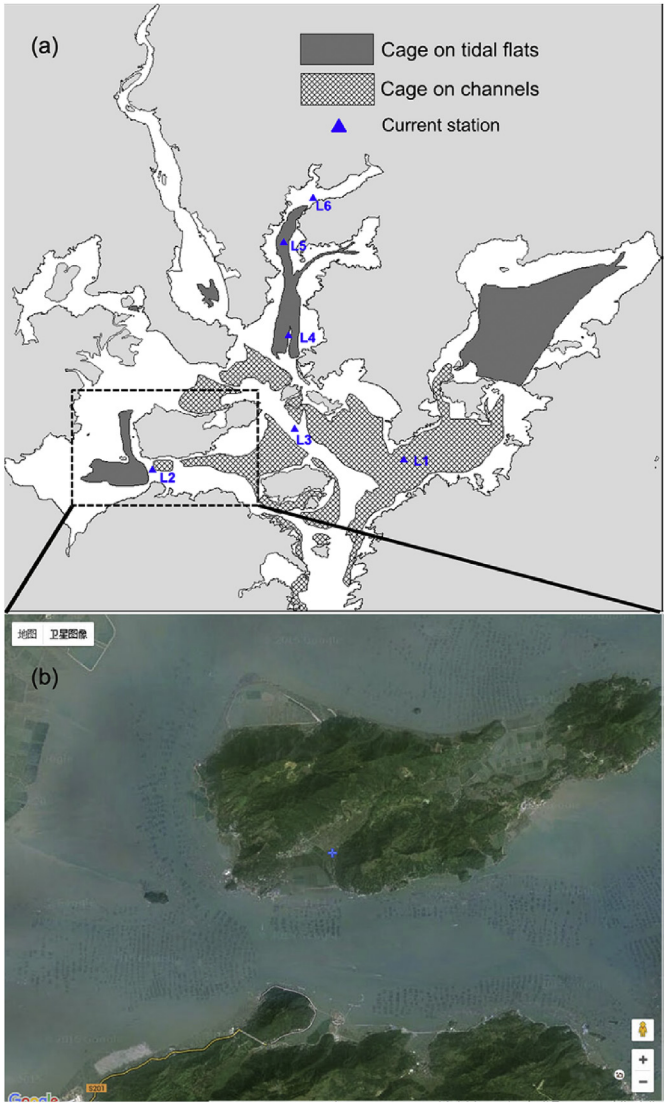

Fig. 2. (a) Spatial distribution of cages in Sansha Bay, shaded by dark gray in tidal flats and by grids in channels, respectively (see legend). (b) An example showing how the upper panel is generated: a subregion from Google map showing the realistic distribution of cages (see the dense dark dots in seawater area).

residual water level between the outer and inner bay is more correlated with cross-shore winds (Lin et al., 2017b).

2.2. Cage distribution and structures

The spatial distribution of the cages in Sansha Bay is shown in Fig. 2a, which is acquired by digitizing the Google map of the study region (see Fig. 2b as an example). It is evident that cages are densely populated in Sansha Bay, including both tidal flats (dark gray area) and channels (gray grids). Cages are floating at the sea surface under the help of wood and plastic foam, but they are also mounted to the sea bottom via anchor lines. An example photo of the cage aquaculture in Sansha Bay is shown in Fig. 3a and the schematic of net cage structure is illustrated in Fig. 3b. A typical cage cell has a square shape with the side length of approximately 4–6 m. A number of modeling studies investigate the cage-induced drag with sophisticated methods considering the fluid-structure interactions (e.g., Yao et al., 2016; Chen and Christensen, 2017) or effects caused by waves and currents (e.g., Lader et al., 2003; Kristiansen and Faltinsen, 2015). Klebert et al. (2013) provided a comprehensive review on the hydrodynamics of net cages.

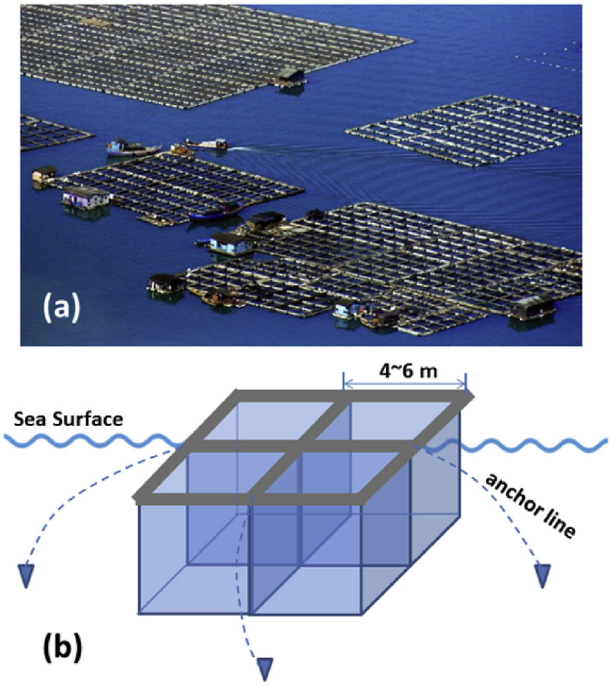

Fig. 3. (a) Example photo of cages in Sansha Bay. (b) Schematic of a typical cage structure in Sansha Bay. The cage is floating at sea surface but mounted to the bottom via several anchor lines.

In this study, we treat the cage-induced drag in a relatively simple way. (i) The cage-induced drag is first estimated by comparisons of current magnitude observed at regions covered by cages and cage-free areas. (ii) Then the cage-induced effect is represented in the numerical model by increasing the local drag coefficient accordingly at areas covered by cages (see Section 5 for details).

3. Methods

In situ hydrographic measurements of Sansha Bay were collected in summer and winter (August 2012 and January 2013) under different tidal conditions (spring and neap tides). Currents were measured at six stations with varying depths (see blue triangles in Fig. 2 for locations). Only winter currents during the spring tide will be used in the present study. During this cruise, currents were first measured simultaneously at the outer three stations (L1, L2 and L3) from January 28 to 29, 2013, and then were measured simultaneously at the inner three stations (L4, L5 and L6) from January 29 to 30, 2013. The current measurements lasted for at least 25 h at each station.

The high resolution shallow water hydrodynamic finite element model (SHYFEM) (Umgiesser et al., 2004) has been used to simulate the wind- and tide-induced processes within the bay. The model, already used with success to simulate processes in lagoons, coastal seas, estuaries and lakes (Umgiesser et al., 2014), adopts the finite element technique and an effective semi-implicit scheme. The wetting and drying processes (Umgiesser et al., 2004) and the transport of tracers (Cucco and Umgiesser, 2006) could also be properly handled by the model. A model setup has been configured specifically for Sansha Bay, which has been proven to be able to reproduce the general hydrodynamic characteristics in the study region (Lin et al., 2017a). For more details about the model setup, we refer to Lin et al. (2017a).

In this study, the model has been used, in concert with observations, to examine the influence of cages on water exchange in Sansha Bay through a few sensitivity runs. In particular, specific simulation runs have been carried out to reproduce the reduction of the flow field induced by the presence of the cages through the local increasing of the

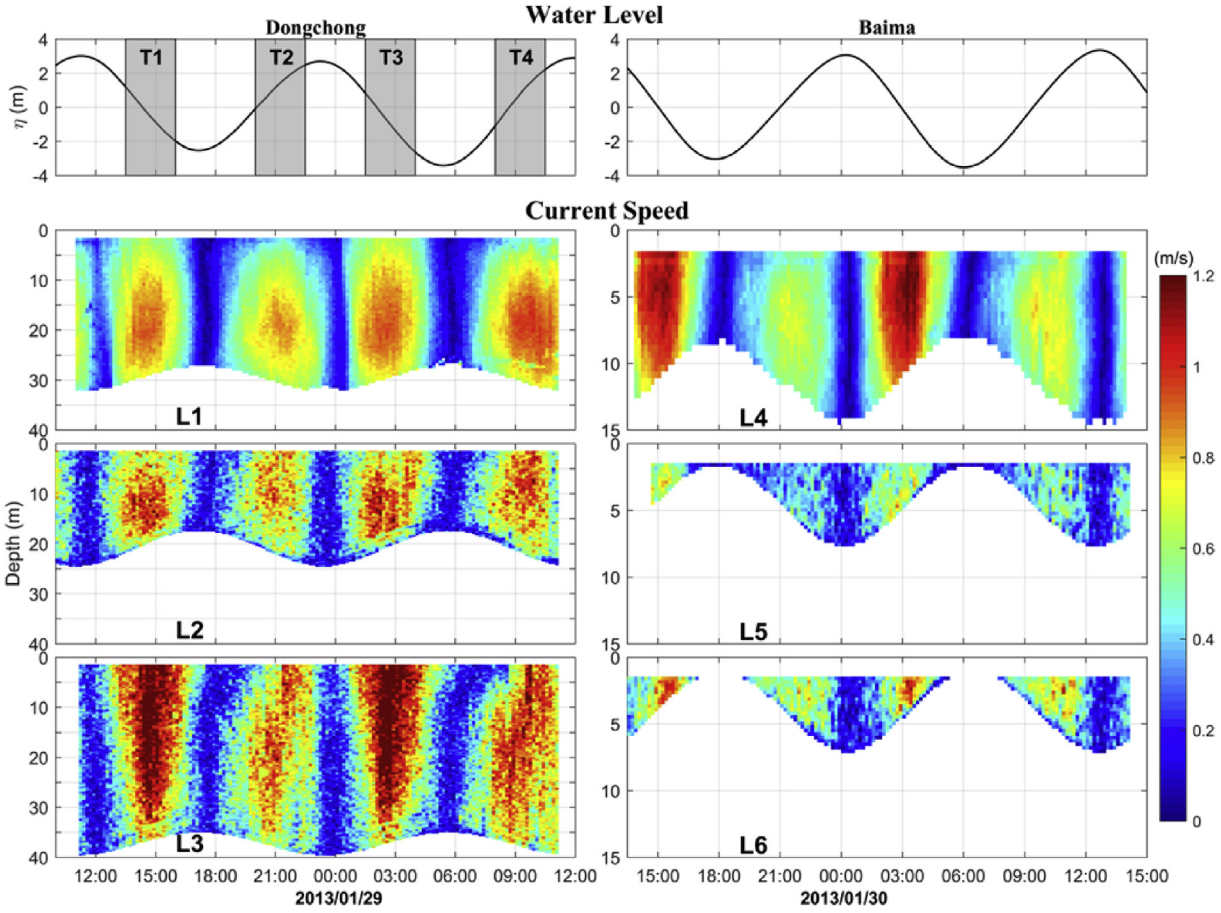

Fig. 4. Water levels (1st row) at stations Dongchong and Baima (see black stars in Fig. 1) and the contemporaneous current speed profiles (2nd – 4th row) observed by shipboard ADCP fixed at six stations (see blue triangles in Fig. 2) during spring tide in winter. The gray shaded bars in the top left panel denote the periods (T1, T2, T3 and T4) when the flood/ebb current speed is stronger, which will be used in Fig. 6. (For interpretation of the references to colour in this figure legend, the reader is referred to the Web version of this article.)

drag factor. Therefore, the indirect effects on the flushing capability were estimated through out the computation of the local water residence times for each simulated configuration.

4. Observed impact of cage aquaculture on water exchange

4.1. Observed flow field

According to the map of cage distribution in Sansha Bay (Fig. 2), some of our current stations are located within the cage areas (L1 and L5), while some other stations are in cage-free areas (L3 and L6). This enables us to compare the flow fields with and without the impact of the cage aquaculture.

The observed current speeds at the six stations, as well as the nearby water-level time series, during winter spring tide are shown in Fig. 4. In order to achieve the simultaneity of current and water-level measurements and hence to examine their relative phases, currents observed at L1, L2 and L3 are compared with water levels at Dongchong station, and currents measured at L4, L5 and L6 are compared with water levels at Baima station (see black stars in Fig. 1 for location of water-level stations). In fact, due to the limited area of Sansha Bay, the phase lag between water levels at bay head (Baima) and bay mouth (Dongchong) is shorter than 20 min. Both water-level and current measurements clearly verify that Sansha Bay is dominated by semi-diurnal tides, as mentioned above (Lin et al., 2017b). In addition, current measurements also suggest that there is a tidal asymmetry in current speeds, with a dominance of ebb tide over flood tide in Sansha Bay. This is particularly evident at stations L3, L4 and L6 (Fig. 4), where the flow field is less influenced by cages.

4.2. Cage-induced drag

Without cage influence, the flow is roughly homogeneous in the vertical except a bottom Ekman layer due to friction. There is no clear indication of surface Ekman layer at these stations, suggesting a limited role of wind on modulating regional currents. Lin et al. (2017b) also found that water-level variability in Sansha Bay was mainly driven by tides instead of winds. For stations within cage areas (e.g., L1, L5), the surface current is clearly weaker than its subsurface counterpart (Fig. 4). To quantify the frictional effect due to cages, we compare the near-surface current speeds for stations within the cage and non-cage areas (Fig. 5). The cage-induced friction could be parameterized by $|\tau_f| = \rho C_D \mathbf{u}^2$, where ρ is the density of seawater, C_D is the drag coefficient, and $\mathbf{u}$ is velocity. It is plausible to assume in Sansha Bay that pressure gradient force is balanced by frictional force and that pressure gradient force is spatially uniform over the entire bay (Jackson and Winant, 1983). Hence the drag coefficient increased by the cage is inversely proportional to the current speed squared.

In order to minimize the influence of spatial inhomogeneity of currents on the differences in the vertical current structures, we compare the current profiles in the same type of regions (channels or tidal flats). Specifically, we separately compare the near-surface squared current speeds with and without the cage-induced frictional effect in channels (L1 vs L3) and tidal flats (L5 vs L6). For relatively deep areas (channels), near-surface current speed squared at L3 (without cage) is larger than that at L1 (with cage) typically by a factor slightly

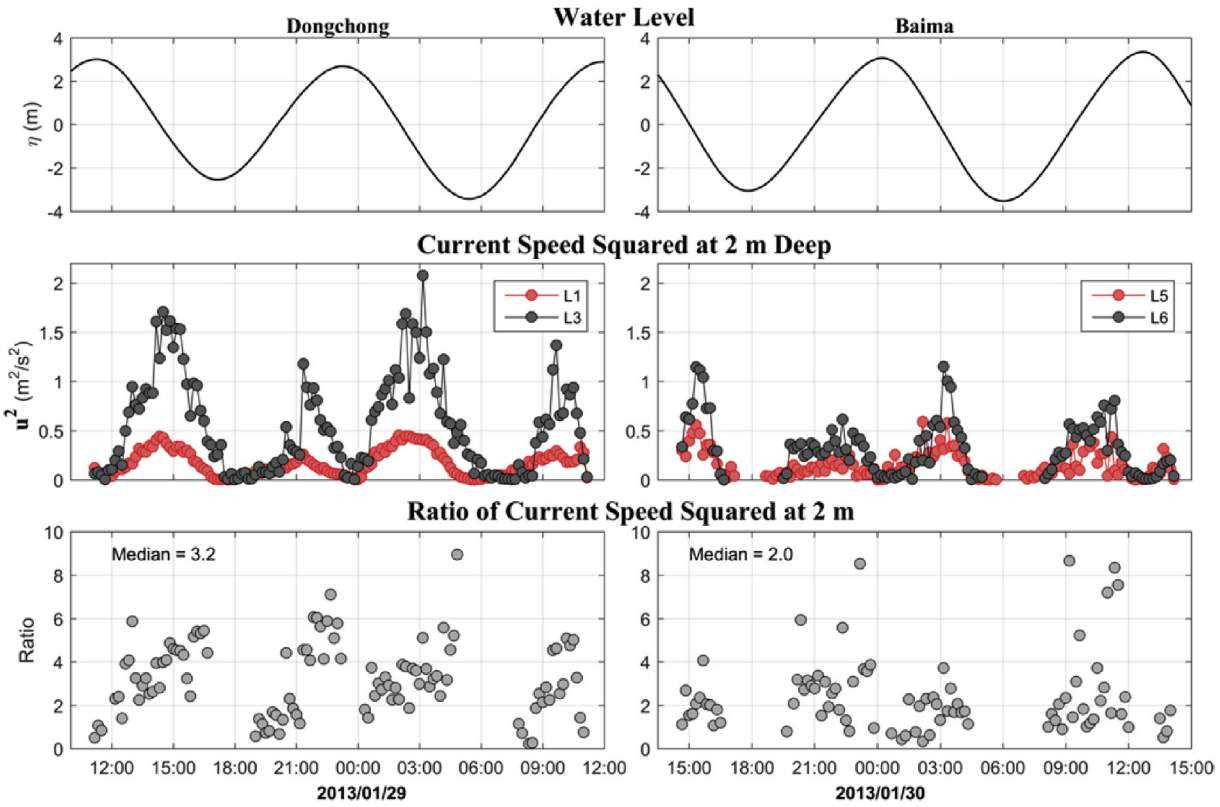

Fig. 5. Comparison of near-surface current speeds with and without the frictional effect due to cages (L1 vs L3; L5 vs L6). (top) Water levels at Dongchong and Baima; same as Fig. 4; (middle) Current speed squared at 2 m depth for stations located within cage (red) and cage-free (gray) areas; (bottom) ratio of the above gray values over red values. The ratio is calculated only when both current speeds are stronger than 0.2 m s^{-1}. (For interpretation of the references to colour in this figure legend, the reader is referred to the Web version of this article.)

exceeding three (Fig. 5, left panels). The situation is slightly more complicated in shallower areas (tidal flats). When the water depth is shallow enough, it is possible that the entire water column could be retarded by bottom friction. One consequence is that the cage-induced drag near sea surface might have a smaller effect than it was supposed to. This is partially evidenced by observations shown in Fig. 5 (right panels). The 2-m current speed squared at L6 is larger than that at L5 typically by a factor of about two, significantly smaller than the ratio in the deeper area. One may speculate that in addition to the reason mentioned above (i.e., bottom friction slows down the water column systematically), this smaller ratio might also be due to the fact that water depth at L6 is itself shallower than that at L5 and hence the flow at L6 is exposed to stronger bottom drag. However, we find that the near-surface current speed squared at L4 is also larger than that at L5 by a factor of only about two (not shown). We thus conclude that cage-induced drag in shallower regions (e.g., tidal flats) is indeed smaller than that in deeper areas (e.g., channels).

We now examine how deep the cage can influence the flow and how the cage-induced drag changes with depth. We pick up current speed profiles at four periods (T1, T2, T3 and T4; Figs. 4 and 6) when the flood/ebb current speed is not too small to avoid singularity of current speed ratios. Cage-induced drag is clearly seen in profiles at L1: current speeds increase gradually with depth in the upper 20 m, but turn to decrease with depth below 20 m due to bottom friction (2nd row, Fig. 6). Without the influence of cages, on the other hand, current speeds at L3 are almost unchanged with depth in the upper 20 m; below 20 m they also decrease toward bottom due to friction (3rd row, Fig. 6). The maximum current speeds (at ~20 m) at L1 are generally smaller than that at L3, possibly because water depth at L1 is shallower than at L3, which results in overlapping of the surface frictional layer and the bottom Ekman layer at L1. According to the profiles shown above, the ratio of current speed squared at L3 against L1 consequently decreases with depth in the upper layer. It is shown that the ratio decreases from larger than three at near surface to about unity at 20 m (4th row, Fig. 6). This implies that cage-induced drag on the flow field in the relatively deep-water channels of Sansha Bay can reach as deep as 20 m, with the drag decreasing with depth. The decreasing rate is however different for different flood/ebb tide periods (see the different slopes of the black lines in the upper 20 m; 4th row, Fig. 6).

5. Simulated impact of cage aquaculture on water exchange

5.1. Different drag coefficients for sensitivities

Based on the comparison of flow fields within cage and cage-free areas, the influence of cage aquaculture on water exchange in Sansha Bay is then investigated using the SHYFEM model. A set of sensitivity runs with different drag coefficients were conducted and the flushing capability of the bay was also estimated. In the model, the bottom friction is parameterized by a quadratic form, $\boldsymbol{\tau_b} = \rho C_D |\mathbf{u}|\mathbf{u}$. C_D is set to be 0.0025 for non-cage area according to previous studies (e.g., Jackson and Winant, 1983; Shi and Wei, 2009).

For areas with cages (shaded areas in Fig. 2a), six sensitivity runs are configured (Table 1). (i) The control run (also termed as Case 0) does not include any cage in the model domain, i.e., C_D is set to be 0.0025 in both cage and cage-free areas. (ii) Case 1: C_D is set to be 0.005 in cage areas, i.e., two times greater than that in cage-free areas. (iii) Case 2: C_D is set to be 0.01 in cage areas, i.e., four times greater. (iv) Case 3: C_D is set to be 0.005 for cage areas in tidal flats (dark gray areas in Figs. 2a), and 0.01 for cage areas in channels (grid areas in Fig. 2a). (v) Case 4: C_D is set to be 0.01 for cage areas in tidal flats and 0.005 in channels. (vi) Case 5: C_D is set to be 0.0025 for cage areas in tidal flats

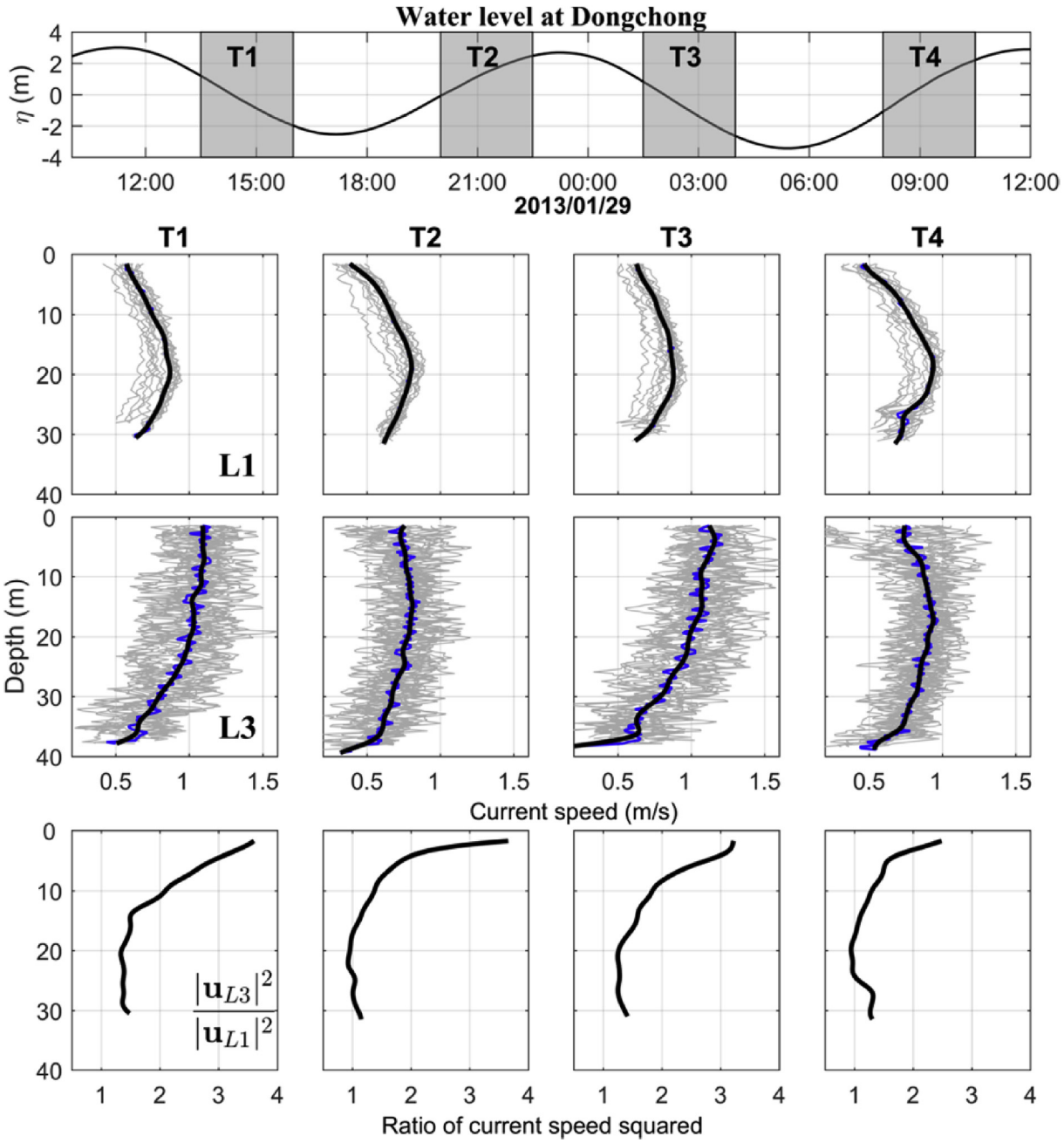

Fig. 6. Profiles of current speed at stations L1 and L3. (1st row) Water level at Dongchong; same as Fig. 4. (2nd row) Current speed profiles at L1 for the four periods T1–T4. The gray curves are the current speed profiles at individual time steps; the blue curve is the median at each layer for the period, and the black curve is the (vertically) 5-m lowpass of the blue curve. (The blue and black curves are almost overlapped for L1.) (3rd row) Same as the 2nd row but for L3. (4th row) Ratio of current speed squared at L3 and L1, namely squared of the ratio of the black curve in the 3rd row against the black curve in the 2nd row. (For interpretation of the references to colour in this figure legend, the reader is referred to the Web version of this article.)

Table 1
Drag coefficient (C_D) in cage areas for different sensitivity runs.

Case	C_D for cages in tidal flats	C_D for cages in channels
Case 0 (control run)	0.0025	0.0025
Case 1	0.005	0.005
Case 2	0.01	0.01
Case 3	0.005	0.01
Case 4	0.01	0.005
Case 5	0.0025	0.02

and 0.02 in channels.

Cases 1 and 2 are designed to investigate the effects of C_D changes on the model results. The observations show that the current speed squared in cage-free areas is larger than in cage areas by a factor exceeding three in channels and about two in tidal flats (Fig. 5). Thus Case 3 represents the real situation. In Case 4, we double the C_D value in tidal flats but halve it in channels compared to Case 3, while in Case 5 the opposite is applied, i.e., double the C_D value in channels but halve it in tidal flats. Cases 4 and 5 are to test the effects of increasing/reducing the population density of cages in channels versus tidal flats on the entire flow fields. This will allow us to evaluate whether reducing cages in tidal flats or in channels is more efficient to enhance the overall

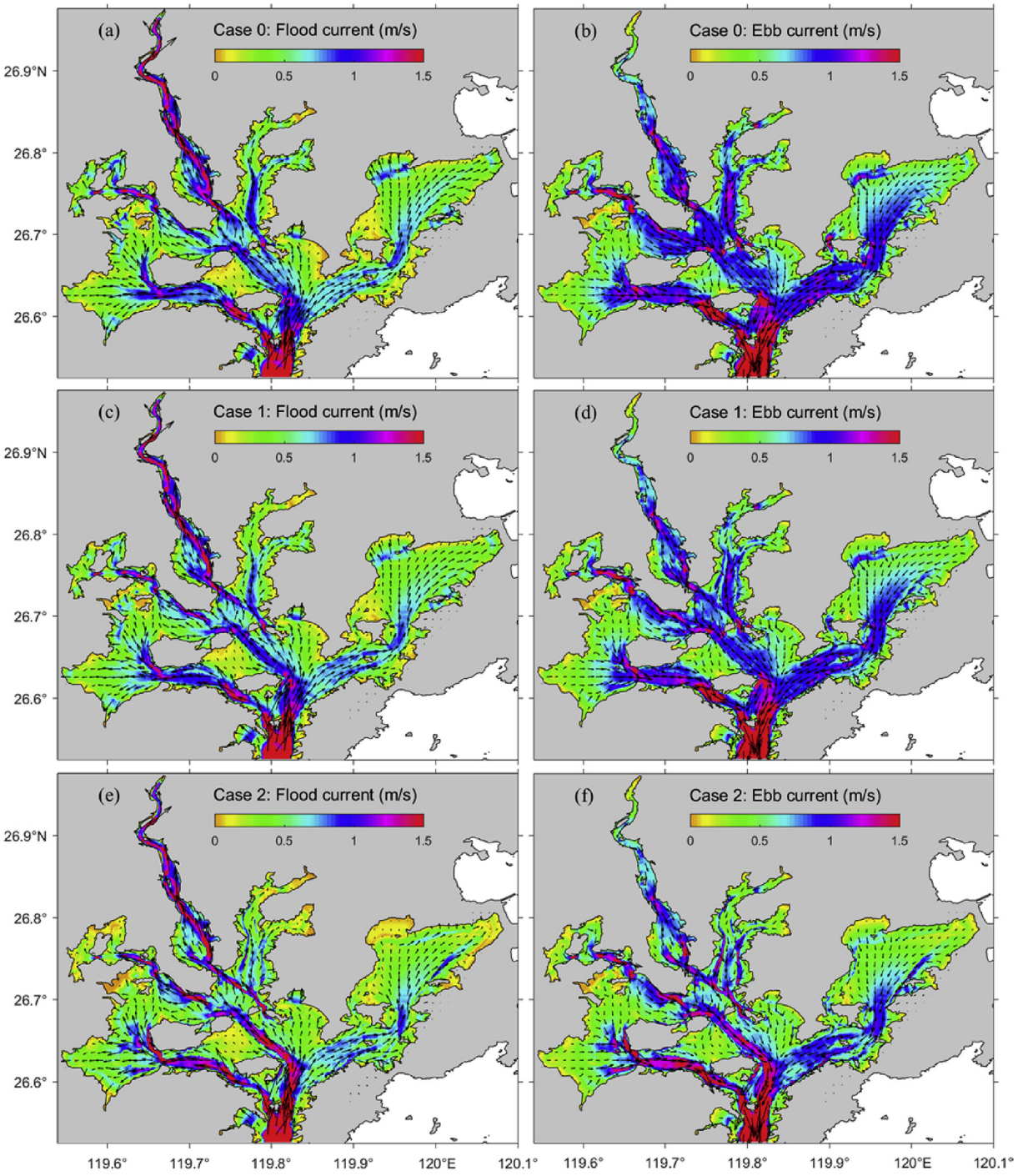

Fig. 7. Simulated fields of (left) flood- and (right) ebb-tide currents in Sansha Bay for different cases.

water-exchange capability in Sansha Bay.

5.2. Impact on flow fields

The simulated flow fields for flood tide and ebb tide are shown in Fig. 7 for the control run and five sensitivity runs. Although the magnitude of current speed differs at certain locations, the general pattern of the current field is similar for different cases. For example, the deeper channels are associated with stronger currents whereas the shallower tidal flats are associated with weaker flows. Sea water flows primarily along main channels with reversing directions during flood and ebb tides, and the ebb-tide currents are generally stronger in magnitude than the corresponding flood-tide currents (Lin et al., 2017a).

Increasing the drag at regions where cages are present results in changes in the flow fields accordingly. Specifically, the relatively strong current streams get narrower but slightly more intense when the drag is increased at cage areas, particularly for the ebb-tide current fields (Fig. 7). The impact of cage-induced drag on the flow field is clearer by examining the speed differences between the control run and the sensitivities (Fig. 8). Combining Fig. 8 and the spatial distribution of cages (Fig. 2), it is evident that the current magnitudes are reduced at cage areas, both in tidal flats and deep channels. Areas with narrow and intensified currents (the red filaments in Fig. 8) are in fact aligned with the gaps of cages (white areas in Fig. 2). This implies that the cage

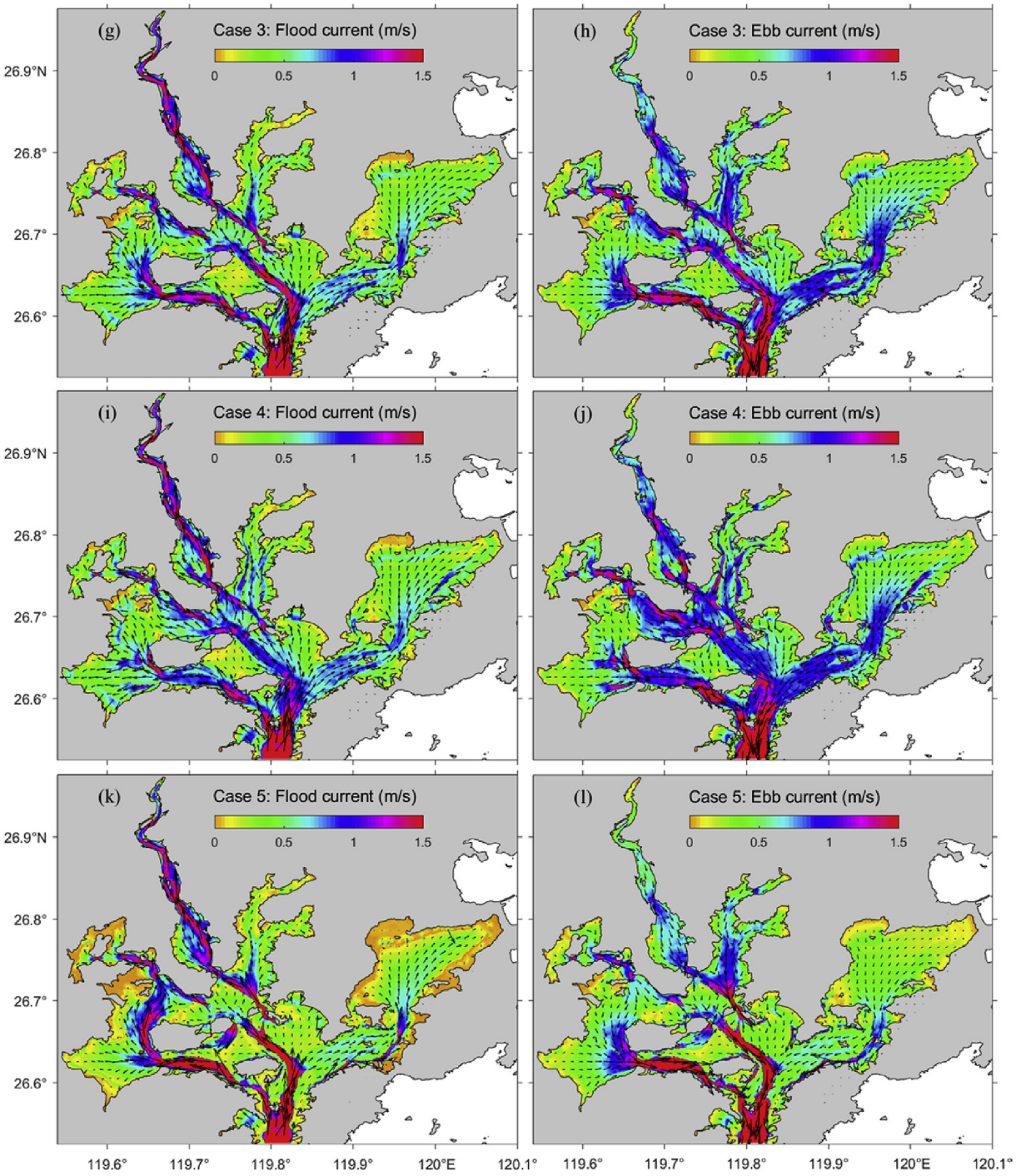

Fig. 7. (*continued*)

aquaculture could reduce the flow locally but increase the flow magnitude adjacent to cages. It is worthwhile to verify in future with observations that whether this is a realistic phenomenon or just a numerical artifact due to the model setting on drag coefficients.

In terms of the specific cases, increasing the drag coefficient (C_D) at cage regions by a factor of two typically reduces the current speed by approximately 0.05 m s^{-1} (Fig. 8a–b), and increasing C_D by a factor of four typically reduced the currents speed by 0.15 m s^{-1} (Fig. 8c–d). Increasing C_D by different times at tidal flats and channels reduces the local current speed by about the similar magnitudes (Fig. 8e–h). Nonetheless, significant increases in C_D at channels (by a factor of eight for Case 5) not only weaken the local currents but also reduce the flow at tidal flats considerably (Fig. 8i–j).

5.3. Impact on half-exchange time

In addition to the direct comparisons of flow fields, the water-exchange capability of Sansha Bay with outside is quantified by the half-exchange time (T_h), which is defined by the time required for half of the sea water within the bay to be replaced by sea water from the open sea under the influence of tidal and residual currents (Cucco and Umgiesser, 2006). The distribution of T_h for the control run (without any cages; Fig. 9) suggests that T_h in the main channels (< 10 d) is generally shorter than that in bay heads (> 30 d). Sea water in the vicinity of Guanjingyang and Dongchong Channel exchanges at a relatively high rate with the open sea, both with $T_h < 5$ d. By contrary, sea water in Baima Harbor has a rather low exchange rate ($T_h > 40$ d)

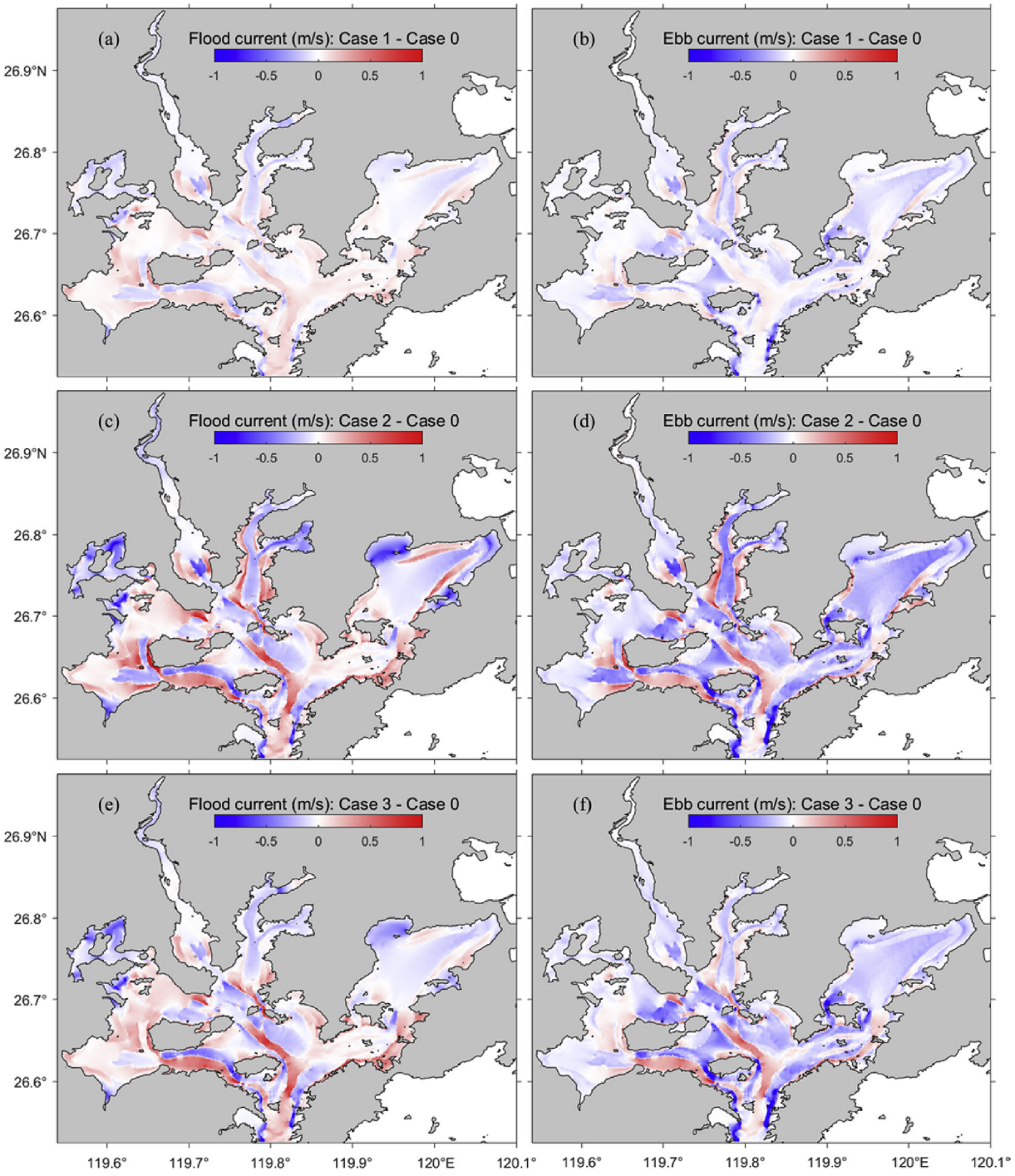

Fig. 8. Differences in flow speed between the control run and the sensitivity runs for (left) flood- and (right) ebb-tide currents.

with the open sea water because it has the longest distance to the bay mouth and also the ebb-tide currents in this harbor are weak and without clear outward residual currents (Lin et al., 2017a). We note that river runoff is not included in the numerical runs here, which might affect the real T_h in Baima Harbor where the Saijiang River is located, but the overall pattern is quite similar. T_h in the eastern bay head of Dongwuyang also exceeds 40 d, possibly due to the weak tidal currents and the inward residual current in this area (Lin et al., 2017a).

Distributions of T_h for the five cases are shown in Fig. 10. The overall pattern of T_h for different configurations of C_D is similar to the control run (compare Fig. 9 and left panels of Fig. 10), i.e., smaller T_h in areas near Dongchong Channel and larger T_h in secondary bays. Increasing C_D by a factor of two in cage areas (Case 1) results in an increment of T_h by less than 10 d in general (Fig. 10b), while increasing C_D by a factor of four (Case 2) leads to a significant increase of T_h in the study region, typically by 10–20 d (Fig. 10d). In particular, the increment of T_h in Yantian Harbor and Dongwuyang exceeds 20 d, due to the extraordinarily dense population of cages in these two secondary bays (Fig. 2a). No apparent increase of T_h is seen along Dongchong Channel and the western part of Guanjingyang, probably due to the stronger currents in this area. The current speed during ebb tide in the vicinity of Dongchong Channel can reach 1.5 m s^{-1} (Lin et al., 2017a), exchanging water rather efficiently between the bay and the open sea.

If we set C_D in tidal flats to be two times, and C_D in channels to be

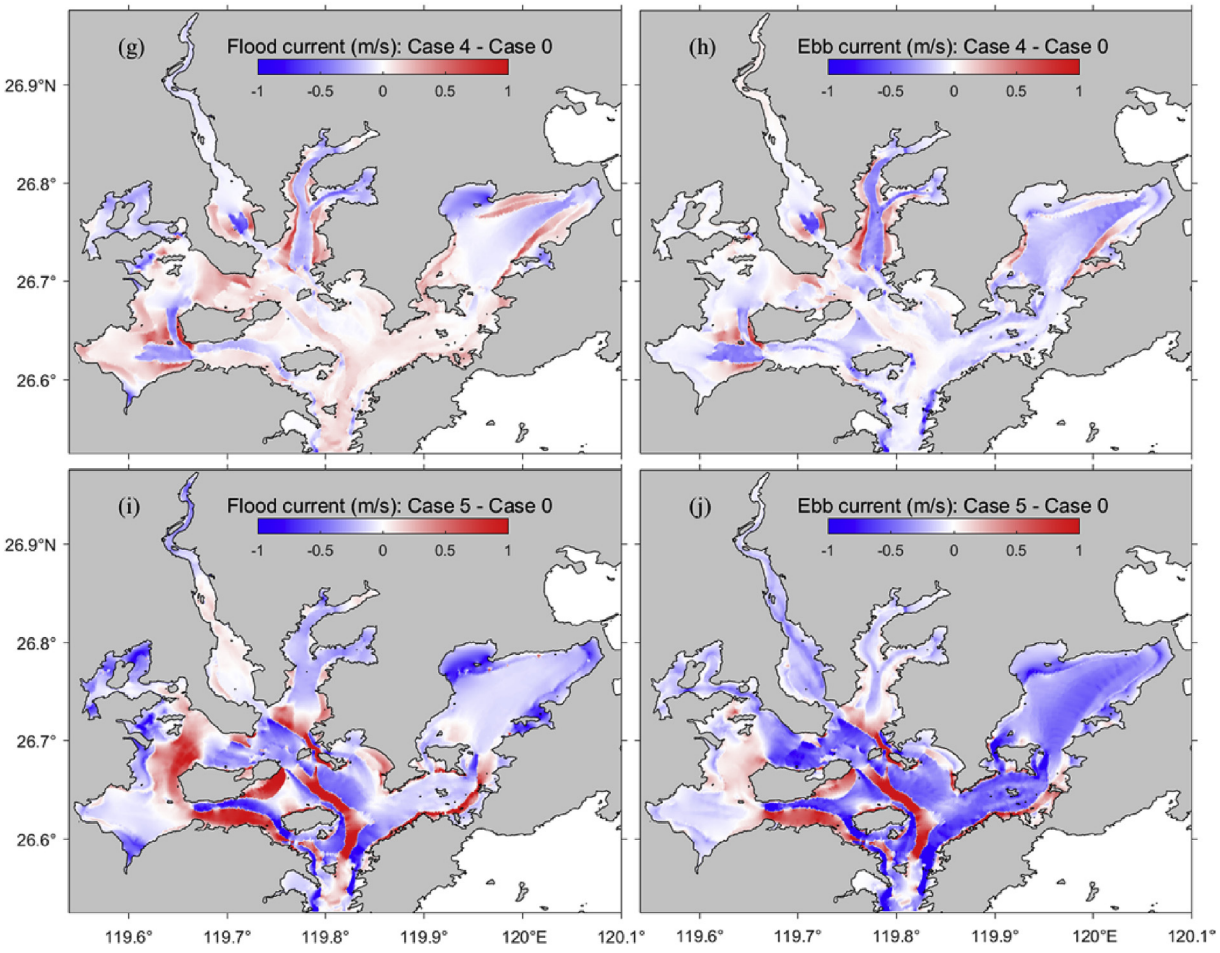

Fig. 8. (*continued*)

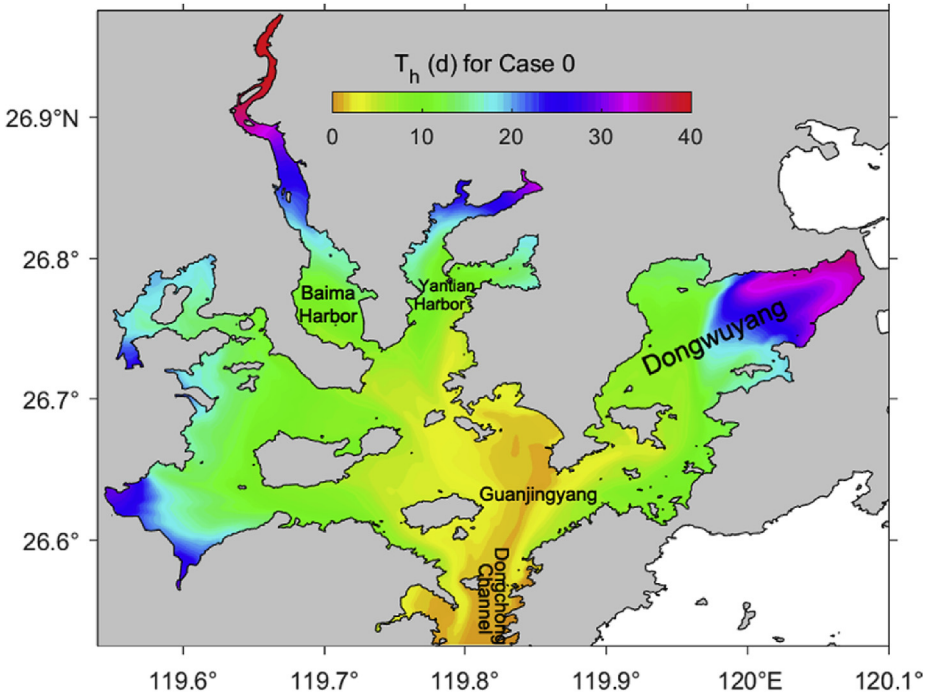

Fig. 9. Distribution of the half-exchange time for the control run (without cages).

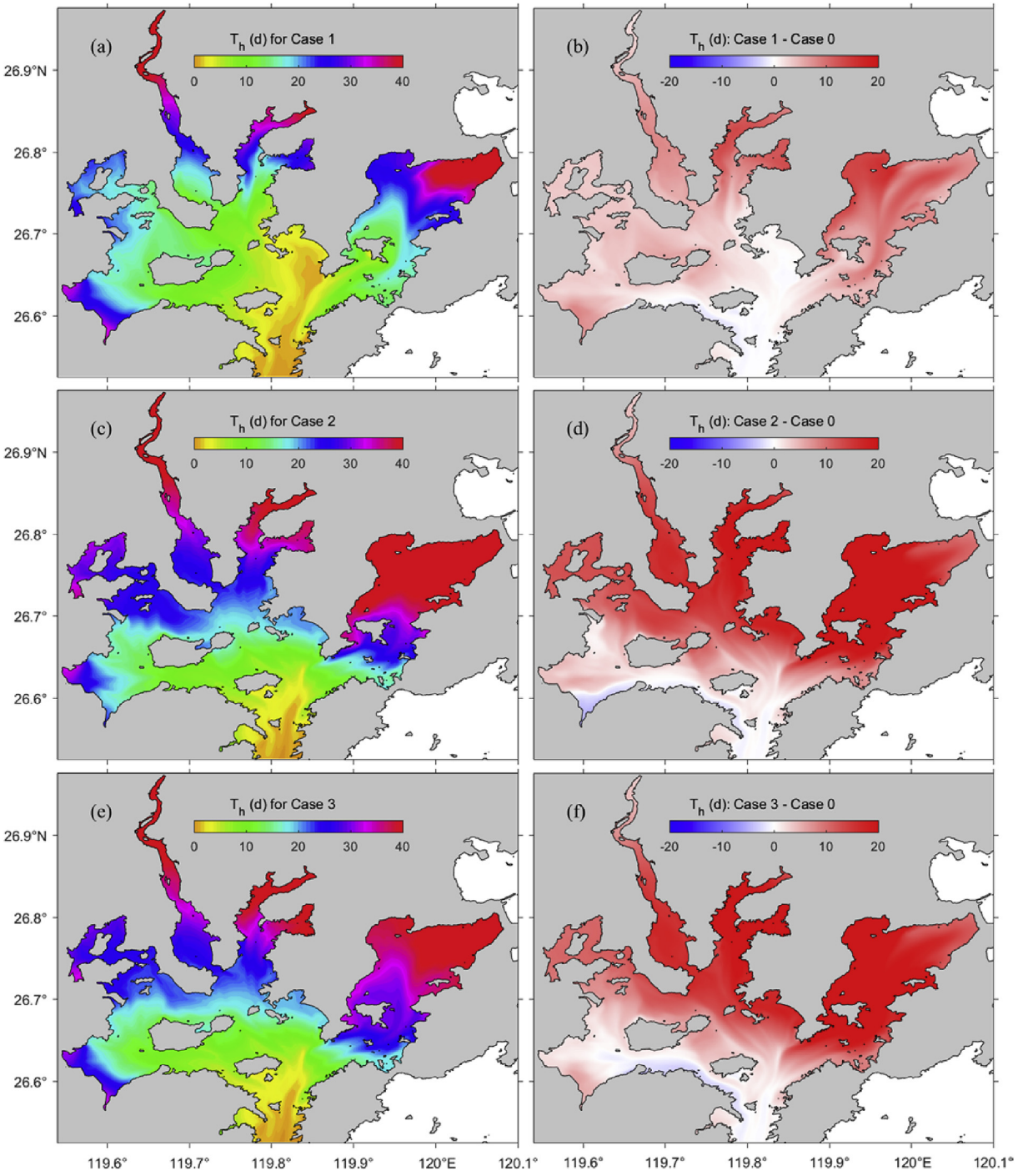

Fig. 10. Distribution of half-exchange time for (left) sensitivity runs and (right) the differences compared with that of the control run.

four times, greater than that in cage-free area (Case 3, or the real situation), the distribution of T_h is quite similar to that of Case 2 (Fig. 10d and f). By doubling the C_D value of Case 3 in tidal flats and halving it in channels (Case 4), T_h is systematically reduced compared to that of Case 3 by about 10 d (Fig. 10f and h). Interestingly, T_h of Case 4 in tidal flats is also smaller than that of Case 3, even though the corresponding C_D is higher in Case 4. By doubling the C_D value of Case 3 in channels and halving it in tidal flats (Case 5), changes in the pattern and values of T_h are minor (typically $<$ 5 d).

If we have to keep the total cages unchanged, Case 4 is equivalent to moving cages from channels to tidal flats; in Case 5, however, we essentially remove cages in tidal flats but significantly increase the drag in channels. It is clear that the overall water-exchange capability of Case 4 is much stronger than that of Case 5 (Fig. 10h and j). This implies that reduction or rearrangement of cages in deep channels of Sansha Bay would be more effective in terms of improving the water-exchange capability of the entire bay.

5.4. Impact on pollutant migration

We also simulate the migration of pollutant using an advection and diffusion module in the model (see Lin et al. (2017a) for model equations), in order to more vividly visualize the impact of cage aquaculture on water exchange and hence the water quality in Sansha Bay. The

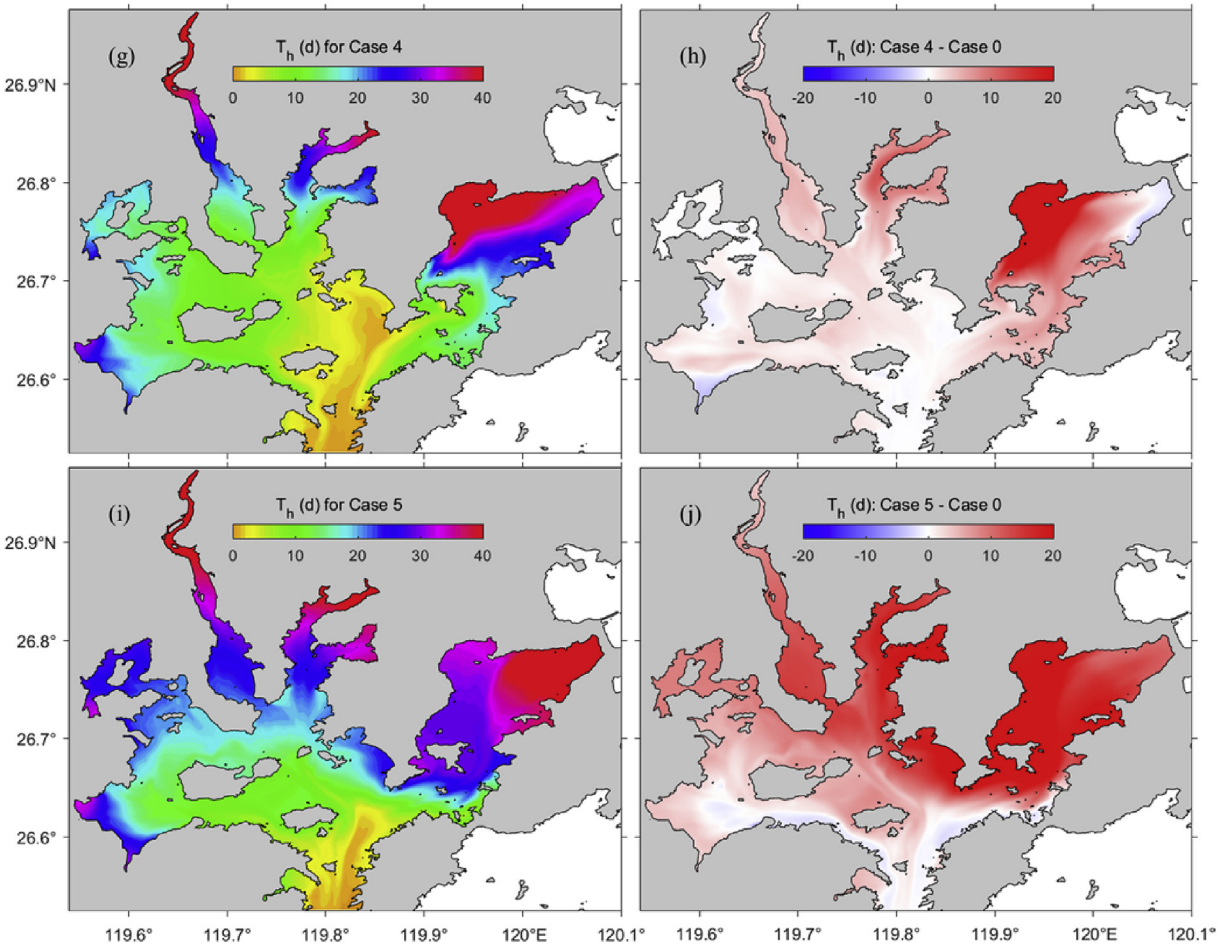

Fig. 10. (*continued*)

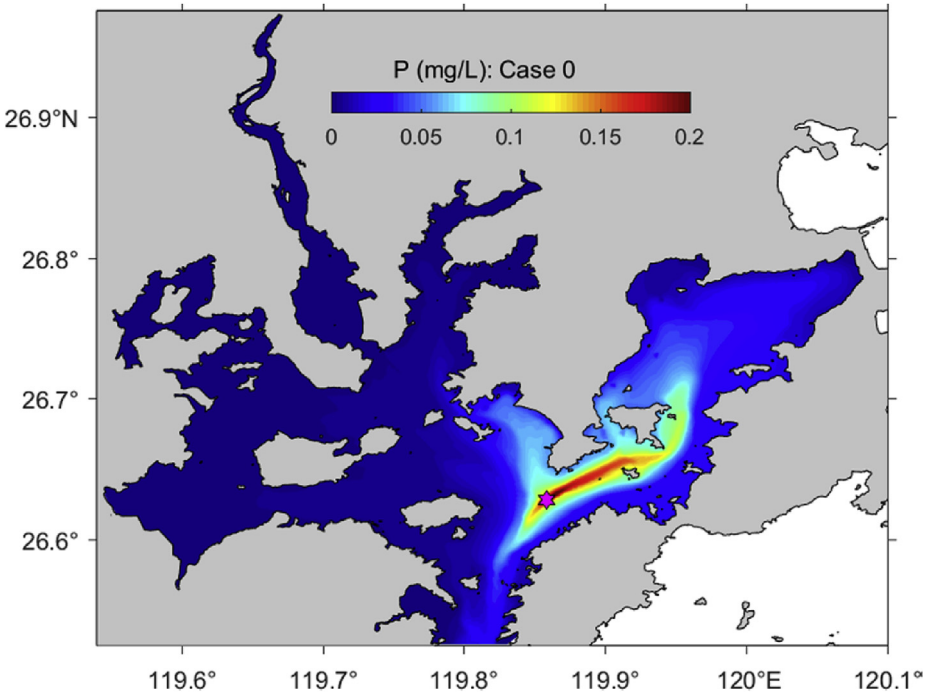

Fig. 11. The envelope of the influenced region by discharged pollutant over a month for the control run. (See the main texts for the meaning of the envelope map.) The magenta hexagram denotes the source point.

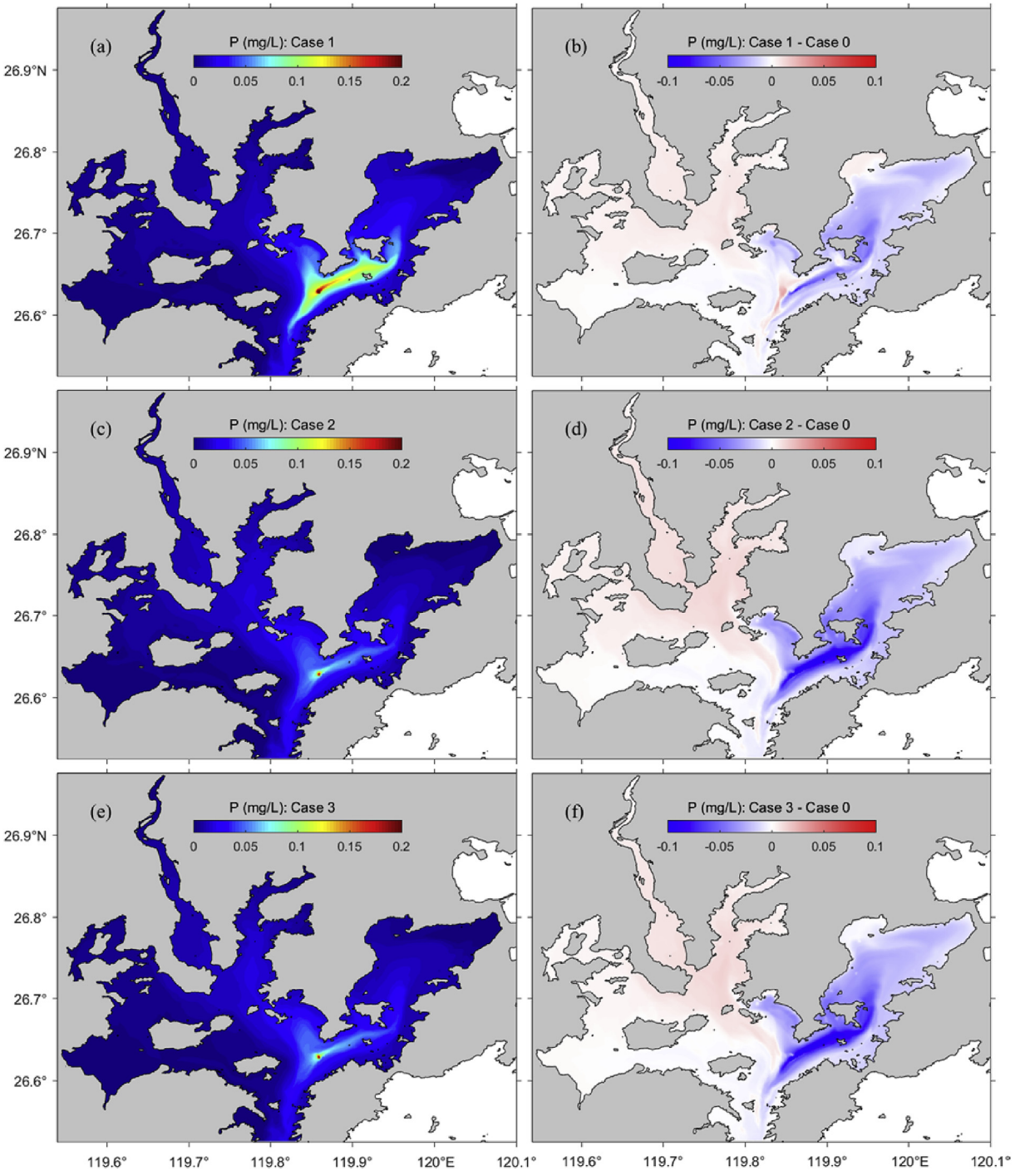

Fig. 12. The envelope of the influenced region by discharged pollutant over a month for (left) sensitivity runs and (right) the differences compared with that of the control run.

major sources of pollutant in Sansha Bay come from river input and cage aquaculture. Hence we choose one location at cage regions in the channel of Guanjingyang as an example pollutant source, and simulate the pollutant migration features by specifying typical values of source intensity and discharge flux. This is also applied to different cases with varying values of C_D (mimicking different cage distribution at tidal flats and channels). In the model the pollutant is discharged with a source concentration of 100 mg L^{-1} and a flux of 1 m^3 s^{-1}.

Once discharged, the pollutant normally diffuses quickly to a rather low value in the vicinity of the source point. So it is less informative to illustrate the distribution of instantaneous or averaged pollutant concentration. Instead, the so-called envelope of the influenced region is often shown, in which a certain contour means the boundary of the maximum area where the pollutant concentration could reach this contour value over a certain period of time. The envelope for the control run over a month (Fig. 11) shows that the high-concentration area is structured as a relatively narrow belt extending from the source point (Guanjingyang) northeastward to the near mouth of Dongwuyang. The western part of Sansha Bay is less affected by the pollutant discharged at Guanjingyang. Overall the pollutant migration and its influence areas are generally consistent with the pattern of tidal currents in the vicinity of the source point.

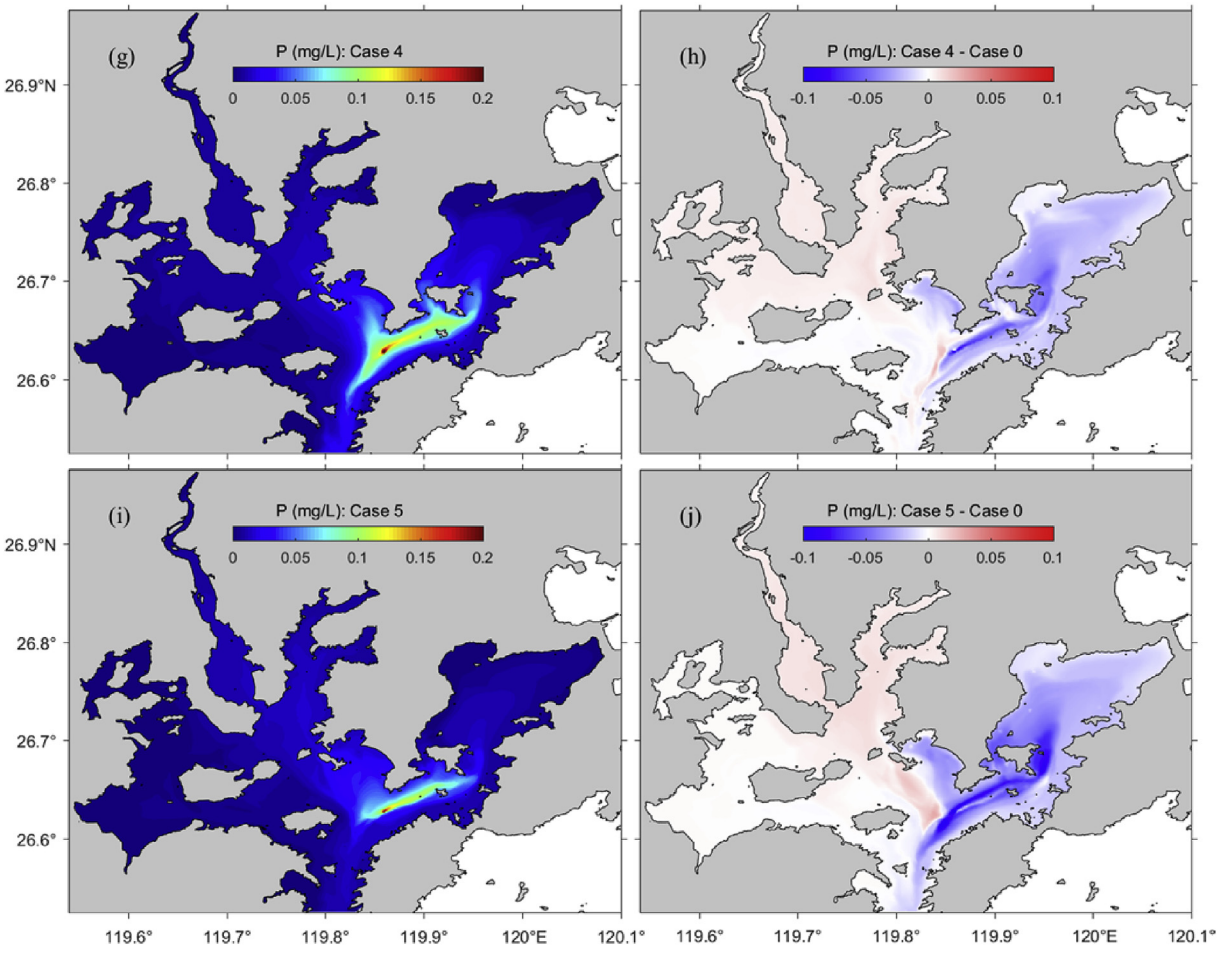

Fig. 12. (*continued*)

Increasing C_D by a factor of two (Case 1) at cage regions slightly reduces the extent of the influenced envelope, but the overall pattern is similar to that of the control run (Fig. 12a–b). Increasing C_D by a factor of four (Case 2) significantly suppresses the spread of pollutant and hence the pollutant high concentration is restricted to the source point over a considerable period of time after discharge. Similar to comparisons in the flow fields and half-exchange time, the map of pollutant influenced envelope for Case 3 is similar to that of Case 2, whereas the map for Case 4 is more similar to that of Case 1 (Fig. 12e–h). The map for Case 5 somehow lies in between the above two groups, showing a high-concentration filament from the source point to the mouth of Dongwuyang (Fig. 12i–j). The sensitivities of pollutant migration imply that attenuated water exchange seems to suppress the spread of pollutant. So pollutant migration for Cases 2 and 3 is more restricted compared to Cases 1 and 4, since the latter two cases have higher water flushing rates. However, smaller frictional drag in Cases 1 and 4 is equivalent to fewer cages and thus less loading of pollutant source. In other words, although the discharged pollutant in Cases 1 and 4 has a larger spread compared to Cases 2 and 3, the source concentration is actually lower which nonetheless was set to be constant (100 mg L^{-1}) for all cases.

6. Conclusions and discussion

The influence of cage aquaculture on the flow field and water exchange in Sansha Bay is investigated based on *in situ* current measurements and output from the SHYFEM model. The observations indicate that the flow in Sansha Bay is relatively uniform in the vertical in cage-free areas, where there is a bottom Ekman layer but no surface boundary layer. This implies that flow in Sansha Bay is driven primarily by tides instead of by winds. Tidal asymmetry is also observed in current measurements with the ebb-tide currents stronger than flood-tide currents.

Near-surface current speed squared in cage-free area is typically larger than that within cage area by a factor exceeding three in deep channels, and by a factor of two in tidal flats. The smaller ratio is possibly due to the overlapping of surface boundary layer and the bottom Ekman layer in shallower cage regions, reducing the drag exerted by the surface cages. Further examination of current speed profiles suggest that cage-induced drag on the flow field can reach as deep as 20 m in the relatively deep-water channels of Sansha Bay.

According to the comparison of observed flow fields within cage and cage-free areas, a set of numerical sensitivity runs with different drag coefficients (C_D) are designed to quantify the impact of cages in tidal flats and channels on water exchange. The results suggest that increasing C_D by a factor of two (four) reduces current speed by approximately 0.05 (0.15) m s^{-1}. Flows at areas within the gaps of cages turn out to be intensified. In other words, cage aquaculture weakens the local flow but strengthens the flow adjacent to cages. In terms of residence time, increasing C_D by a factor of two (four) leads to an increase of the half-exchange time (T_h) typically by < 10 d (10–20 d). The increment of T_h in tidal flats is significantly larger than that in channels, due to the dense population of cages and weaker currents in tidal flats. Reducing C_D in the relatively deep channels significantly decreases T_h not only locally, but also in the tidal flats. Therefore, certain clearance or rearrangement of cages in channels could more effectively improve the water exchange in Sansha Bay as a whole. The simulations of pollutant migration suggest that retarded water exchange is also

accompanied by suppressed pollutant spread. However, lower drag at channels means fewer cages and hence less pollutant source loading. So even though fewer cages at channels lead to more rapid flushing rate and hence larger spread of pollutant, the source concentration is actually lower.

The influence of cages is represented in the model by simply increasing the drag coefficient to a single value. In reality, however, differences in for example cage shape and aquaculture species are possible to induce contrasting impacts on the local flow field. Therefore, discriminating representations of cages in the model are potentially required in the next step to consider the frictional stresses induced by the existence of cages.

Acknowledgments

This study is supported by the National Key R&D Program of China (No. 2018YFC1406302), the Public Science and Technology Research Funds Projects of Ocean (No. 201205009-2), the National Natural Science Foundation of China (Nos. 41606009, 91858201 and 41890801), Xiamen University Fundamental Research Funds for the Central Universities (No. 20720180099), and Laboratory for Regional Oceanography and Numerical Modeling, Pilot National Laboratory for Marine Science and Technology (Qingdao) (No. 2017A02). We appreciate the insightful comments from two reviewers that improve an early version of the manuscript.

References

Chen, H., Christensen, E.D., 2017. Development of a numerical model for fluid-structure interaction analysis of flow through and around an aquaculture net cage. Ocean. Eng. 142, 597–615.

Cucco, A., Umgiesser, G., 2006. Modeling the venice lagoon residence time. Ecol. Model. 193 (1), 34–51.

Edwards, P., 2015. Aquaculture environment interactions: past, present and likely future trends. Aquaculture 447, 2–14.

Ferreira, J.G., Saurel, C., Lencart e Silva, J.D., Nunes, J.P., Vazquez, F., 2014. Modelling of interactions between inshore and offshore aquaculture. Aquaculture 426–427, 154–164.

Herrera, J., Cornejo, P., Sepúlveda, H.H., Artal, O., Quiñones, R.A., 2018. A novel approach to assess the hydrodynamic effects of a salmon farm in a Patagonian channel: coupling between regional ocean modeling and high resolution les simulation. Aquaculture 495, 115–129.

Holmer, M., Marbá, N., Terrados, J., Duarte, C.M., Fortes, M.D., 2002. Impacts of milkfish (Chanos chanos) aquaculture on carbon and nutrient fluxes in the Bolinao area, Philippines. Mar. Pollut. Bull. 44 (7), 685–696.

Holmer, M., Wildish, D., Hargrave, B., 2005. Organic enrichment from marine finfish aquaculture and effects on sediment biogeochemical processes. In: Hargrave, B. (Ed.), Environmental Effects of Marine Fish Aquaculture. Handbook of Environmental Chemistry. Springer-Verlag, Berlin, pp. 181–206.

Jackson, G.A., Winant, C.D., 1983. Effect of a kelp forest on coastal currents. Cont. Shelf Res. 2 (1), 75–80.

Klebert, P., Lader, P., Gansel, L., Oppedal, F., 2013. Hydrodynamic interactions on net panel and aquaculture fish cages: a review. Ocean. Eng. 58, 260–274.

Kristiansen, T., Faltinsen, O.M., 2015. Experimental and numerical study of an aquaculture net cage with floater in waves and current. J. Fluids Struct. 54, 1–26.

Lader, P.F., Enerhaug, B., Fredheim, A., Krokstad, J., 2003. Modeling of 3D net structures exposed to waves and current. In: Third International Conference on Hydroelasticity in Marine Technology, vols. 15–17 September 2003, Oxford, UK.

Lin, H., An, B., Chen, Z., Sun, Z., Chen, H., Zhu, J., Huang, L., 2016. Distribution of summertime and wintertime temperature and salinity in Sansha Bay. J. Xiamen Univ. 55 (3), 349–356 (in Chinese with English abstract).

Lin, H., Chen, Z., Hu, J., Cucco, A., Zhu, J., Sun, Z., Huang, L., 2017a. Numerical simulation of the hydrodynamics and water exchange in Sansha Bay. Ocean. Eng. 139, 85–94.

Lin, H., Hu, J., Zhu, J., Cheng, P., Chen, Z., Sun, Z., Chen, D., 2017b. Tide- and wind-driven variability of water level in Sansha Bay, Fujian, China. Front. Earth Sci. 11 (2), 332–346. https://doi.org/10.1007/s11707-016-0588-x.

Liu, J., Zheng, Q., Chen, H., Yu, Z., Lin, Y., 2003. Water quality condition in Sansha bay. J. Oceanogr. Taiwan Strait 22 (2), 201–204 (in Chinese with English abstract).

Naylor, R.L., Golburg, R.J., Primavera, J.H., et al., 2000. Effect of aquaculture on world fish supplies. Nature 405, 1017–1024.

San Diego-McGlone, M.L., Azanza, R.V., Villanoy, C.L., Jacinto, G.S., 2008. Eutrophic waters, algal bloom and fish kill in fish farming areas in Bolinao, Pangasinan, Philippines. Mar. Pollut. Bull. 57, 295–301.

Shen, L., Li, C., Wu, X., Gong, L., Hao, S., 2014. Temporal and spatial variation characteristics of inorganic nitrogen and active phosphorus and relations with environmental factors in Sansha Bay of Fujian in summer and winter. J. Appl. Oceanogr. 33 (4), 553–561 (in Chinese with English abstract).

Shi, J., Wei, H., 2009. Simulation of hydrodynamic structures in a semi-enclosed bay with dense raft-culture. J. Ocean Univ. China 39 (6), 1181–1187 (in Chinese with English abstract).

Shi, J., Wei, H., Zhao, L., Yuan, Y., Fang, J., Zhang, J., 2011. A physical-biological coupled aquaculture model for a suspended aquaculture area of China. Aquaculture 318, 412–424.

Sun, P., Yu, G., Chen, Z., Hu, J., Liu, G., Xu, D., 2015. Diagnostic model construction and example analysis of habitat degradation in enclosed bay: iii. Sansha Bay habitat restoration strategy. Chin. J. Oceanol. Limnol. 33 (2), 477–489. https://doi.org/10.1007/s00343 -015-4169-8.

Udarbe-Walker, M.J., Magdaong, E., 2003. Circulation and hydrographic characteristics of a mariculture area, NW of Lingayen Gulf. Philipp. Sci. 40, 57–72.

Umgiesser, G., Canu, D.M., Cucco, A., Solidoro, C., 2004. A finite element model for the Venice Lagoon. Development, set up, calibration and validation. J. Mar. Syst. 51, 123–145.

Umgiesser, G., Ferrarin, C., Cucco, A., De Pascalis, F., Bellafiore, D., Ghezzo, M., Bajo, M., 2014. Comparative hydrodynamics of 10 Mediterranean lagoons by means of numerical modeling. J. Geophys. Res. Oceans 119 (4), 2212–2226.

Wang, Y., Song, Z., Jiang, C., Kong, J., Liu, Q., 2009. Numerical and Environmental Studies of Bays in Fujian Province – Sansha Bay (In Chinese). Ocean Press, Beijing, pp. 283pp.

Weitzman, J., Steeves, L., Bradford, J., Filgueira, R., 2019. Far-field and near-field effects of marine aquaculture. In: Sheppard, C. (Ed.), World Seas: an Environmental Evaluation. Academic Press, pp. 197–220.

Wu, H.Y., Chen, K.L., Chen, Z.H., Chen, Q.H., Qiu, Y.P., Wu, J.C., Zhang, J.F., 2012. Evaluation for the ecological quality status of coastal waters in East China Sea using fuzzy integrated assessment method. Mar. Pollut. Bull. 64, 546–555.

Yao, Y., Chen, Y., Zhou, H., Yang, H., 2016. Numerical modeling of current loads on a net cage considering fluid–structure interaction. J. Fluids Struct. 62, 350–366.

Zhu, F., Shi, Z., Ling, X., Xia, Y., Li, Y., Weng, Y., Liu, Y., 2013. Relationship between cage aquaculture and environmental quality in Sansha Bay of Ningde. Mar. Sci. Bull. 32 (2), 171–177 (in Chinese).